Self-Trapped Excitons in LH2 Antenna Complexes between 5 K and Ambient Temperature

Arvi Freiberg,*,†,‡ Margus Rätsep,† Kõu Timpmann,† Gediminas Trinkunas,§ and Neal W. Woodbury‡

Institute of Physics, University of Tartu, Riia 142, Tartu 51014, Estonia, Department of Chemistry and Biochemistry and Center for the Study of Early Events in Photosynthesis, Arizona State University, Tempe, Arizona 85287, and Institute of Physics, Savanoriu pr. 231, LT-2053 Vilnius, Lithuania

Received: February 26, 2003; In Final Form: July 31, 2003

High-spectral-resolution hole-burning and fluorescence line-narrowing spectra of excitons in LH2 complexes from the photosynthetic purple bacterium *Rhodobacter sphaeroides* have been investigated together with conventional broadband fluorescence spectra and their temperature dependence. The steady-state spectroscopy has been complemented by fluorescence lifetime measurements. The experimental results are discussed on the basis of the adiabatic Holstein exciton polaron model, modified by including diagonal disorder. As a result, a new interpretation for the LH2 antenna optical spectra is provided. The exciton when optically excited becomes localized after relaxation. The LH2 fluorescence is mainly due to self-trapped excitons not only at low temperature, as previously suggested (Timpmann, K.; Katiliene, Z.; Woodbury, N. W.; Freiberg, A. *J. Phys. Chem. B* **2001,** *105,* 12223), but also over the whole temperature range up to physiological temperatures because the self-trapped exciton binding energy is of the same order as the thermal excitation energy at ambient temperature. The conclusion is made that direct self-trapping relaxation dominates the common energy relaxation between exciton states and that the main factor limiting the relaxed exciton size is dynamic rather than static disorder. The coexistence of large and small exciton polarons at low temperatures has been confirmed. Exciton self-trapping also essentially modifies the long-wavelength tail of the absorption spectrum of LH2 complexes. The fraction of the absorption spectrum that is subject to hole burning is due to large-radius self-trapped excitons that are weakly coupled to the lattice. The rest of this spectrum that survives hole burning belongs to the strongly coupled self-trapped excitons/excimers. Implications of these results on the interpretation of Stark spectroscopy experiments as well as on photosynthetic energy transfer and trapping are discussed.

Introduction

All photosynthetic processes start with the absorption of light by an antenna pigment complex. For maximum efficiency, light energy must be absorbed over a broad range of wavelengths and then delivered via energy transfer to the reaction center where photochemical energy transduction takes place. Despite active research, there is still a considerable lack of knowledge concerning precisely how nature has managed this formidable task. (See refs 1 and 2 for a review.) We believe that one key to answering this question is a better understanding of the nature of the excited states of the antenna pigment−protein complexes created by light.

Probably the best studied of all antenna complexes, both structurally[3,4] and functionally,[5] is the peripheral LH2 (light-harvesting 2) antenna complex from purple nonsulfur bacteria. The LH2 antenna is made up of a circular arrangement of polypeptide heterodimers (α and β subunits). Each heterodimer contains three bacteriochlorophyll *a* (Bchl) molecules. Two of the three Bchl's in each heterodimer are closely attached and in the larger structure form a ring of coupled Bchl dimers. The optical properties of the LH2 complex have been studied in some detail using a broad variety of techniques. (See ref 1 for a comprehensive review.) It is well established that the ring of

Bchl dimers seen in the structure absorbs near 850 nm (hence the band designation B850), and the remaining Bchl's absorb near 800 nm (B800). Both of these spectral bands are derived from the Q_y singlet electronic transition observed in Bchl molecules. Low-temperature hole burning[6,7] and single-complex studies[8,9] provided unambiguous proof that in large ensembles the absorption and emission spectra of LH2 complexes are inhomogeneously broadened. A large downshift of the 850-nm band relative to the one at 800 nm has conveniently been explained by strong dipolar exciton coupling between the closely packed B850 pigments, which are absent in the looser B800 assembly. This interpretation is in line with different circular dichroism spectra of B800 and B850.[10,11]

In the following discussion, we shall mainly concentrate on B850 excitons, which determine the functionally important flow of excitation energy in the photosynthetic membrane between the peripheral LH2 antenna complexes as well as that from the LH2 to the core LH1 antenna complexes. Structural and optical spectroscopy data together have led to the development of a disordered circular exciton model for the B850 aggregate.[11−13] The main spectroscopic features of this model that is well represented by various experimental studies are as follows. With vanishing disorder and owing to the specific orientation of the transition dipoles of Bchl molecules that are almost in the B850 ring plane, the B850 absorption spectrum is dominated by two degenerate transitions, $k = \pm 1$ (k is the quantum number proportional to the exciton quasi-momentum). The third transition, $k = 0$, has the lowest energy and is optically almost

* Corresponding author. E-mail: freiberg@fi.tartu.ee. Phone: +372-7-383024. Fax: +372-7-383033.
† University of Tartu.
‡ Arizona State University.
§ Institute of Physics, Vilnius.

forbidden. Disorder causes a lifting of the degeneracy, a modification of the spacing between the levels, and a redistribution of the oscillator strength among different transitions so that not only the $k = 0$ transition but also a few higher-energy ($k > 1$) transitions gain appreciable intensity.

A distribution of narrow (about 1 cm^{-1} wide) persistent spectral holes has been observed at the low-energy tail of the B850 absorption band upon burning with a monochromatic laser beam.[12,14] The narrow holes are accompanied by much broader (100−200 cm^{-1}) holes at higher energies. The distribution of narrow holes, designated B870, is believed to represent the distribution of zero-phonon origins corresponding to the $k = 0$ transitions in an inhomogeneous ensemble of B850 excitons. Intense zero-phonon holes are accompanied by weak phonon sidebands less than 20 cm^{-1} away from the zero-phonon hole, suggesting a weak coupling of the $k = 0$ excitons to lattice vibrations. The broad holes have been assigned to the upper exciton states broadened by fast interexciton state relaxation down to the lowest exciton state. Direct femtosecond time-resolved studies have indeed shown an ultrafast response of the system within the first 100 fs after optical excitation.[15,16] (See ref 5 for a review.) Together, these observations have been taken as a confirmation of the validity of the disordered exciton model in describing the spectroscopy (and dynamics) of B850 excitations.

Several observations, however, seem to challenge certain aspects of this model. Given the ultrafast inter-exciton-state relaxation to the lowest $k = 0$ exciton level and the small optical reorganization energy (resulting from the weak exciton−phonon coupling and small characteristic phonon frequency), one would expect to observe a resonant fluorescence with only a very small red (or Stokes) shift from the B870 states at low temperatures. No such resonant exciton fluorescence has been found so far. The LH2 emission spectrum is broad and considerably red-shifted compared to the maximum of the B870 band under any excitation condition.[17] Spectrally selective excitation within the B870 band results in only minor fluorescence band narrowing[17,18] suggesting that exciton−phonon coupling for the transition from the relaxed excited state must be strong. The ensemble data are corroborated with the single-molecule measurements, which show broad fluorescence spectra, albeit with greatly varying shapes for different complexes.[8] An analysis of the linear and nonlinear absorption spectra of LH2 using a disordered exciton model[19] reveals another set of problems. It is easy to show on the basis of this model that within the limits of commonly accepted exciton coupling energy, $200 \leq J \leq 500$ cm^{-1}, it is impossible to satisfy simultaneously the three most important parameters determined from the hole-burning experiment: (i) the position of the B870 band relative to that of the B850 absorption band; (ii) the B870 bandwidth; and (iii) the integral intensity of the B870 band relative to that of B850. In general, a better compromise between different experimental data is achieved if larger inhomogeneous broadening is assumed. This is probably why most researches refer to relatively large spectral disorder. It is also notable that the model in its canonical form fails to explain the low-temperature fluorescence excitation spectra of single LH2 complexes. This led to the postulation of a permanent elliptical deformation of the B850 ring.[9]

To reconcile some of the above controversies, it has been suggested recently that the emitting exciton states of LH2 must qualitatively differ from most of the absorbing states.[17] We have modeled this using the concept of a self-trapped exciton.[17,20] What this amounts to is that in the deformable lattice an exciton may be trapped by the lattice deformation created by its own presence, provided the exciton−lattice interaction is sufficiently strong. This phenomenon is called self-trapping. (See ref 21 for a review.) A characteristic spectroscopic effect of self-trapping is a broad emission band red-shifted relative to a more structured absorption band.

In this work, evidence for exciton self-trapping in LH2 complexes over the whole temperature range from 5 K to ambient temperatures is presented. The study combines high-spectral-resolution hole-burning and fluorescence line-narrowing investigations applicable at low temperatures with conventional broadband spectroscopy and picosecond time-resolved fluorescence lifetime measurements at higher temperatures. Experimental data are complemented with theoretical analysis based on the adiabatic Holstein polaron model including both static and dynamic disorder. As a result, physical parameters characterizing exciton polarons in the B850 aggregate have been evaluated. Others have discussed related aspects of the antenna polaron model.[22−26]

Experimental Section

Sample Preparation and Characterization. LH2 complexes from *Rhodobacter (Rb.) sphaeroides* were prepared as described earlier.[27] The samples were diluted with 20 mM Tris-HCl buffer at pH 8.0 containing 1 mM EDTA and 0.1 M NaCl and with glycerol (1:2 volume ratio) to yield a desired absorbance in the sample cell. In the final solution, the LDAO concentration was increased to ∼1% to maintain the LH2 complexes as well-separated units over long periods of experimental time.

Dynamic light scattering was used to investigate the aggregation state of the LH2 complexes in the sample solution at ambient temperature (25 °C). In this technique, laser light scattered by a diffusing particle is analyzed in terms of the temporal field autocorrelation function. From the known dependence of the correlation function measured over a wide range of times on the diffusion properties of the particles, a distribution of hydrodynamic radii (R_h) of the scattering units can be obtained.[28] In the present case, the commercially available DynaPro-MS/X (Protein-Solutions Inc.) particle-sizing instrument has been utilized. The data (not shown) were dominated (>99% from the overall scattering intensity) by a peak at $R_h = 3.0 \pm 0.5$ nm. Because this is close to the outer-wall radius of the cylindrical LH2 complexes from *Rps. acidophila* determined by X-ray structure analysis,[3] we conclude that our solution contains well-isolated LH2 complexes. A much weaker peak observed at $R_h = 72 \pm 22$ nm has tentatively been assigned to fragments of the photosynthetic membrane remaining after isolation.

Steady-State Spectral Studies. The low-resolution absorption and fluorescence spectra of LH2 complexes were taken using standard techniques. Measurements at low temperatures down to 4.2 K were performed using a liquid-helium cryostat (Utreks, Ukraine) equipped with a temperature-controlling and stabilizing system. Care was taken to avoid fluorescence reabsorption effects on the emission spectra (Figure 1) and lifetime. The LH2 spectra in Figure 1 are recorded in the reflection geometry with respect to the excitation light beam in order to minimize the reabsorption effect. As can be seen from Figure 1, optical densities that exceed ∼0.1 for a 1-cm path length at the absorption band maximum lead to serious distortions of the fluorescence band, including both spectral red shift and broadening. Somewhat less severe effects are expected at low temperatures because of the generally smaller overlap between the absorption and emission spectra.
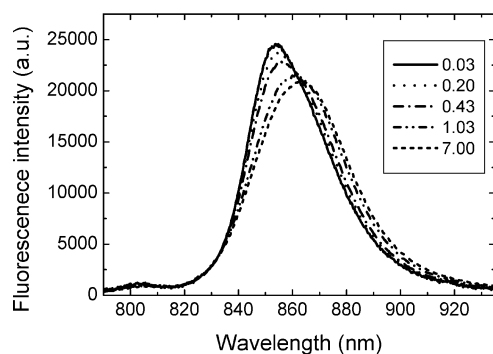
Figure 1. Reabsorption effects on the fluorescence spectrum of isolated LH2 complexes from *Rb. sphaeroides* at room temperature. The measurements have been performed using reflection geometry in a standard 1-cm spectrophotometer cell, except the one at the highest optical density for which a 1-mm-thick cell was used. The given optical density is for the room-temperature maximum of the B850 absorption band at 846.2 nm. Excitation is at 590 nm, resonant with the Q_x absorption band of Bchl molecules. Area-normalized shapes of the fluorescence spectrum at different optical densities are indicated.

A Ti:sapphire solid-state laser (model 3900S, Spectra Physics) pumped by an Ar^+ ion laser (model 171, Spectra Physics) was used for the hole-burning and fluorescence line-narrowing measurements. The Ti:sapphire laser line width was 0.07 cm^{-1}. For transmission measurements, a 12-V tungsten lamp was used. Detection was performed by using a 0.6-m spectrograph (MDR-23, LOMO, Russia) and an electrically cooled CCD camera (Andor Technology). The spectral resolution varied from 0.1 to 0.4 nm depending on the grating used. The wavelength scale of the spectrometer was calibrated to a precision of ± 0.1 nm using a calibration lamp. The emission spectra were corrected to the spectral sensitivity of the apparatus. The burning laser power was adjusted between 4 and 200 mW over about a 1-cm^2 illuminated sample area, and the burn times were varied from 0.5 to 4 min in order to produce proper holes without saturating the sample.

Picosecond Time-Resolved Fluorescence Lifetime Measurements. The picosecond emission spectrometer (picosecond spectrochronograph) that was used has been described in detail.[29] In the present study, it consists of a Coherent 700 styril-9M mode-locked dye laser, synchronously pumped at 76 MHz by a Coherent Antares 76S Nd:YAG laser, as an excitation source with 3−5-ps pulse width, a subtractive-dispersion double-grating monochromator (MDR-2, LOMO, Russia) as a spectral analyzer, and a home-built synchroscan streak camera as a fast detector. The streak camera was linked via a vidicon to an OSA 500 optical spectrum analyzer (B&M Spektronik, FRG). The scattering from the sample at the excitation wavelength was recorded and used as an instrument response function. The typical width of the response function during these measurements was 30 ps.

Experimental Results and Discussion

Broadband versus Line-Narrowed Absorption and Fluorescence Spectra at Low Temperatures. Figure 2a shows steady-state absorption and nonresonantly excited fluorescence spectra of LH2 complexes from *Rb. sphaeroides* at 5 K. Narrow spectral holes can be burned when exciting resonantly in the long-wavelength tail of the absorption spectrum. A distribution of zero-phonon hole depths measured at constant nonsaturating burning fluence is also shown in Figure 2a. The amplitude of the distribution in the Figure is enhanced 20 times for better visibility. This is the so-called hole-burning action spectrum[30] representing the distribution of zero-phonon lines of the
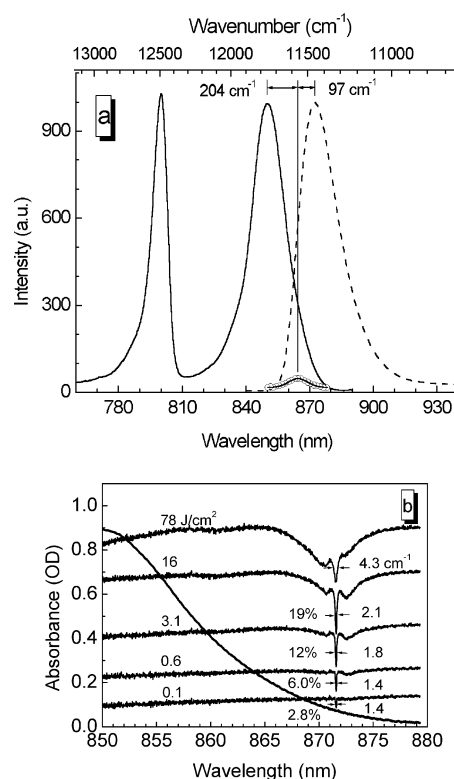

Figure 2. (a) Peak-normalized steady-state absorption and nonselectively excited (at 800 nm) fluorescence spectra of LH2 complexes from *Rb. sphaeroides* at 5 K. The fluorescence spectrum (- - -) with its maximum at 872.2 nm ($11465 \pm 5 \text{ cm}^{-1}$) is corrected for the monochromator transmittance and the photomultiplier sensitivity. The absorption spectrum (—) longer-wavelength maximum is at 849.9 nm ($11766 \pm 5 \text{ cm}^{-1}$). Shown at the red tail of the absorption spectrum is a distribution of zero-phonon hole depths for the B870 band measured at constant burn fluence and normalized to the saturated hole depth. The distribution function is approximated by a Gaussian shape centered at 11562 cm^{-1} (864.9 nm) and having a width of 147 cm^{-1}. (b) Hole-burned spectra at 871.6 nm measured with a resolution of 1.3 cm^{-1} using the different burning laser fluences shown. The curve in the background is the absorption spectrum. The hole spectra are magnified 20 times relative to the absorbance scale and shifted vertically with respect to each other. The fractional hole depths and hole widths are also indicated.

previously mentioned B870 band. The distribution has a nearly Gaussian shape peaking at 864.9 nm (at $11562.0 \pm 5 \text{ cm}^{-1}$, that is $204 \pm 10 \text{ cm}^{-1}$ below the B850 absorption band maximum) and having a $147 \pm 10 \text{ cm}^{-1}$ width (here and below, the spectral width indicates fwhm). The earlier reported numbers for the width and relative band shift are similar: 135 ± 10 and $185 \pm 10 \text{ cm}^{-1}$ in ref 30 and 165 ± 10 and $204 \pm 10 \text{ cm}^{-1}$ in ref 20, respectively. The width of the action spectrum is considered to be a measure of static inhomogeneous spectral broadening. Some variation of the data in different samples was noticed earlier.[30]

Figure 2b shows hole-burning spectra using a 871.6-nm burn wavelength measured as a function of increasing burn laser fluence. The smallest (bottom curve) and the largest (top curve) applied fluence differ by almost 3 orders of magnitude. The narrow dip in resonance with the burning laser line is the zero-phonon hole. Associated with the zero-phonon hole are real and pseudo-phonon sideband holes from the left and right sides, respectively. One can see that there is a gradual broadening of the zero-phonon holes from the experimentally limited value of $\sim 1.5 \text{ cm}^{-1}$ at the lowest fluence to $\sim 4.4 \text{ cm}^{-1}$ at the highest. The zero-phonon hole broadening is accompanied by a relative increase in the sidebands and some change in their shape. The

zero-phonon hole at 871.6 nm starts to broaden at a fractional hole-depth value (defined as the absorbance change divided by the initial absorbance) of ~12% (at a burn fluence of ~3 J/cm^2). By increasing the burning fluence, the hole depth saturates at ~20%. Because of this excitation saturation effect, care should be exercised in determining the Huang−Rhys factor, S, characterizing the linear exciton−phonon coupling strength. It determines the mean number of emitted vibrational quanta upon electronic transition. According to hole-burning theory,[31] the integrated intensity of the zero-phonon hole divided by the intensity of the entire hole profile is equal to $\exp(-2S)$. We have obtained for nonsaturating conditions (the two lowest spectra in Figure 2b) $S = 0.3$, in agreement with ref 12. Combined with the average phonon frequency of 16 cm^{-1}, this leads to a rather small lattice relaxation energy of $E_{LR} \leq 5$ cm^{-1}.

From the other side, one would also expect that the saturated fractional absorbance change at the burn wavelength would be determined by $\exp(-S)$.[31] A value of $S = 0.3$ gives a saturated hole depth of 74%, which is in obvious disagreement with the measured 20% depth of the saturated hole. A straightforward conclusion would be that only a part (20%/0.74 = 27%) of the red-tail absorption at 871.6 nm stems from the lowest-energy B870 states that give rise to narrow zero-phonon holes. If this is the case, then the integrated absorbance of the B870 band (including contributions from both zero-phonon holes and phonon sideband holes) constitutes only 3.4 ± 0.4% of that of the B850 absorption band.

The other possible explanation of the apparent contradiction described above could be that the S value is underestimated for some reason.[32] Assuming a limiting case in which all of the red absorption at the burning wavelength belongs to B870, we find that a fractional hole depth of 20% gives $S = 1.6$. This large S, compatible with strong exciton−phonon coupling, apparently is not consistent with the shape of the hole spectra presented in Figure 2b. We shall return to this issue below.

As outlined in the Introduction, a common interpretation based on the weakly disordered exciton model is that the B870 band represents an inhomogeneous distribution of the lowest-energy $k = 0$ exciton states. One would then expect that the LH2 fluorescence should originate from these states at low temperatures. The spectral shape of this emission using nonselective excitation is easy to simulate, provided that both the inhomogeneous distribution function of the emitting states and the elementary (homogeneously broadened) resonant fluorescence spectrum are known. To account for the latter, we employ the pseudo-phonon sideband of the hole-burning spectrum. In the linear electron−phonon coupling approximation, generally well founded for chlorophyll-like molecules, a mirror image is maintained between the absorption and emission spectra at thermal equilibrium. Therefore, the resonant fluorescence phonon sideband may be expected to have a shape similar to that of the pseudo-phonon sideband in the hole-burning spectrum, at least qualitatively.

Figure 3a demonstrates the resonant fluorescence spectrum obtained by convoluting the B870 band with the elementary fluorescence spectrum, as deduced above. For comparison, the experimental fluorescence spectrum, nonselectively excited at 800 nm (the same as in Figure 2a), is also shown. As seen in this Figure, the estimated nonselectively excited resonance fluorescence is only slightly (by ~15 cm^{-1}) red-shifted relative to the B870 band. This is in striking contrast to the experimental spectrum, which shows a red shift more than 6 times as large, −97 ± 10 cm^{-1}. The experimental band is also much (almost 2 times) broader than the simulated one. We thus conclude that
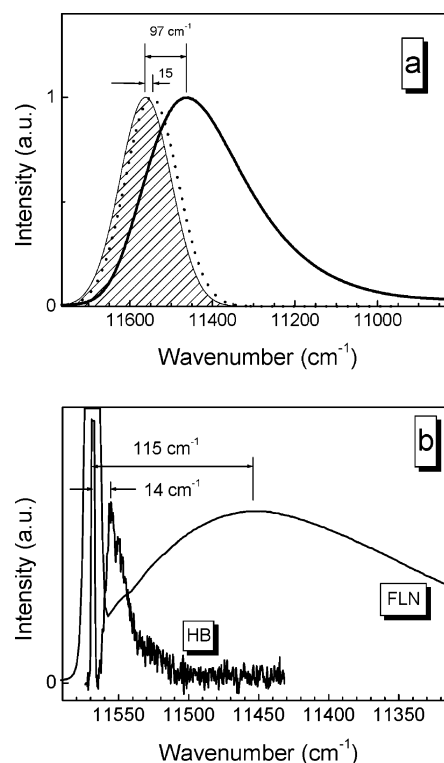

Figure 3. (a) Comparison of the broadband experimental fluorescence spectrum (solid curve, the same as in Figure 2a) of LH2 complexes from *Rb. sphaeroides* at 5 K with the simulated resonant fluorescence spectrum (· · ·). The simulated spectrum is obtained by the convolution of a shaded Gaussian, approximating the inhomogeneous distribution function of zero-phonon holes (the B870 band), with corresponding elementary (homogeneously broadened) fluorescence spectra (see text for details). (b) Comparison of the line-narrowed fluorescence (FLN, excited at 868.5 nm) and hole-burning (HB, burned at 864.5 nm) band shapes of LH2 complexes from *Rb. sphaeroides* at 5 K. The fluorescence spectrum is corrected for the sensitivity of the recording system.

the emission observed at nonresonant excitation does not in its entirety represent the anticipated resonant fluorescence from the B870 states.

Finally, incomplete exciton relaxation might give rise to this apparent inconsistency. If so, then excitation directly into the B870 band should clearly reveal the resonant fluorescence with expected characteristics. This is not the case, as has already been demonstrated.[17,20] Apart from some narrowing, the fluorescence band remains fundamentally red-shifted, broad, and structureless when selectively excited on the red slope of the LH2 absorption spectrum.

Figure 3b compares fluorescence and hole-burning band shapes of B850 complexes at 5 K, both excited close to the maximum of the B870 absorption band and then shifted together according to their origin. For convenience, only the hole-burning pseudo-phonon sideband (representing the anticipated resonant fluorescence phonon sideband) is plotted along with the low-intensity part of the zero-phonon hole. Also, the peak intensity of the phonon sidebands is normalized.

As is evident from this Figure, the profiles of the two spectra differ drastically. The hole-burning sideband maximum is about 8 times closer to the band origin than it is in fluorescence, and its width is almost 16 times narrower. Numerically, the fluorescence bandwidth that is equal to ~286 cm^{-1} using nonselective excitation (Figure 2a) is reduced only slightly, to ~250 cm^{-1}, upon resonant excitation. The energy gap between the excitation laser line and the fluorescence peak is 119 ± 5
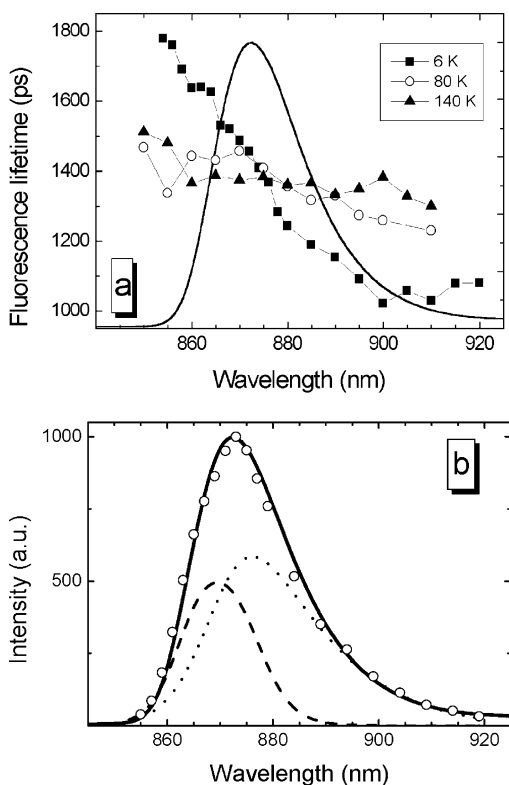
Figure 4. (a) Fluorescence lifetime of LH2 complexes from *Rb. sphaeroides* recorded as a function of emission wavelength and temperature. Nonselective excitation with picosecond pulses at 800 nm is used. The fluorescence spectrum in the background is measured at 6 K. Curves connecting experimental points are shown to aid the eye. (b) Decomposition of the fluorescence spectrum into resonant fluorescence (- - -) and self-trapped exciton emission ($\cdot\cdot\cdot$) components according to eq 1. The steady-state fluorescence spectrum (the same as in Figure 2a) is shown with a continuous curve, and that simulated using the time-resolved fluorescence data, with open dots. See the text for details.

cm^{-1} (determined between 868 and 880 nm and averaged over all experimental data). The latter number can be considered to be an apparent Stokes shift because of the ground-state lattice relaxation accompanying exciton recombination, E_{LR}. Similar albeit less-detailed data have been reported for LH2 complexes from *Rhodospirillum molishianum*[18] and *Rhodopseudomonas acidophila*.[33]

Fluorescence Lifetime as a Function of Emission Wavelength at Low Temperatures. Shown in Figure 4a is the fluorescence decay time measured at three temperatures as a function of the emission wavelength. The fluorescence at each recording wavelength is integrated over a 2−4-nm-wide spectral region (defined by the slit width of the spectrometer), with the exact spectral width depending on the signal intensity. Because of the weakness of the signal at the fluorescence band edges, the optical density of the sample was increased to 0.2 (measured at the absorption band maximum at room temperature).

A strong decay-time dependence on the emission wavelength is seen at 6 K. The lifetime, which is close to 1.8 ns at the blue edge of the spectrum, gradually shortens toward longer wavelengths until it stays constant after reaching ∼1.1 ns at ∼890 nm. This low-temperature spectral dependence, overlooked in our previous study,[17] becomes progressively weaker with increasing temperature and almost disappears above 140 K. The present 80 K data quantitatively agrees with that measured previously at 77 K using a phase-modulation technique.[34] Within the limits of our experimental accuracy, the decay kinetics is single-exponential for all emission wavelengths and temperatures studied (data not shown), and the excitation pulse determines the rise time of the fluorescence signal.

One reason for the spectral dependence of the fluorescence lifetime could be fluorescence reabsorption, yet the reabsorption effect is expected to increase with temperature because of an increasing spectral overlap, in contrast to experimental observations. Another reason could be energy transfer involving both intra- and inter-B850 ring processes. This, however, would result in behavior opposite to what has been observed (i.e., in faster kinetics appearing at shorter wavelengths). In addition, there should be a concomitant fluorescence rise time at longer emission wavelengths with the same time constant measured for the decay of the shorter-wavelength fluorescence, which is also not seen.

Still another possibility is a heterogeneous fluorescence band. On the basis of kinetic measurements, it unfortunately is impossible to determine how many spectral components contribute to the emission band. Therefore, we necessarily consider the simplest case in which only two essentially different spectral subbands (henceforth called blue or RF and red or ST components) are present. We can then evaluate the RF and ST component spectra from the following system of equations:

$$\tau(\lambda) = \frac{\tau_{RF}A_{RF}(\lambda) + \tau_{ST}A_{ST}(\lambda)}{A_{RF}(\lambda) + A_{ST}(\lambda)} \quad (1)$$

$$A_{RF}(\lambda) + A_{ST}(\lambda) = 1$$

where $\tau(\lambda)$ is the measured fluorescence decay time at wavelength λ, $A_{RF}(\lambda)$ and $A_{ST}(\lambda)$ are the fractional spectral amplitudes (the component amplitude divided by the total amplitude of the fluorescence spectrum at wavelength λ) of the components, and τ_{RF} and τ_{ST} are their lifetimes, taken to be independent of the wavelength.

Shown in Figure 4b is the result of such a spectral decomposition using $\tau_{ST} = 1.1$ ns and $\tau_{RF} = 2.1$ ns. Although τ_{ST} is well defined from Figure 4a by the horizontal part of the curve, the real value of τ_{RF} is experimentally uncertain. Fortunately, the shape and position of the RF band depend very little on the choice of τ_{RF}. The RF component spectrum shown in Figure 4b is asymmetric toward longer wavelengths, peaks at 869−870 nm (11508−11494 cm^{-1}), and has a width of 190−255 cm^{-1}. It contributes ∼40% to the total fluorescence spectrum. The ST band is also asymmetric toward longer wavelengths, has a maximum at 874−876 nm (11442−11416 cm^{-1}), and has a width of 300−320 cm^{-1}. It constitutes ∼60% of the overall intensity of the B850 fluorescence band. Considerable uncertainty in those numbers is due to the low spectral resolution used, especially at the fluorescence band edges. However, a fair agreement of the directly recorded steady-state fluorescence spectrum and of that built using the component amplitudes and lifetimes from the fluorescence kinetics measurements (open dots) in Figure 4b leads to confidence in the decomposition procedure used. Taking $\tau_{RF} = 1.8$ ns increases the contribution of the RF component to 47% and shifts the ST band to 878 nm.

One is now tempted to assign the RF component to the resonant fluorescence (explaining the abbreviation used) because of its spectral position close to the B870 absorption band and also because longer lifetimes are expected for the resonant fluorescence because of the partially prohibited nature of the lowest $k = 0$ exciton states.

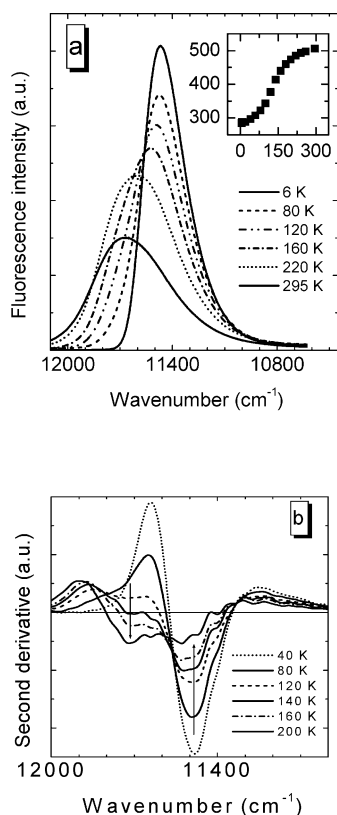Then, to satisfy the RF component bandwidth and its maximum position relative to the B870 band, a Huang−Rhys

Self-Trapped Excitons in LH2

J. Phys. Chem. B, Vol. 107, No. 41, 2003 **11515**

Figure 5. (a) Fluorescence spectra and (b) fluorescence second-derivative spectra of LH2 complexes from *Rb. sphaeroides* at different temperatures. Excitation is at 799 nm, and spectra are corrected for the sensitivity of the recording system. The arrows in panel b indicate the main trends in spectral changes with increasing temperature. The inset in panel a shows the temperature (on the horizontal axis in K units) dependence of the fluorescence bandwidth (on the vertical axis in wavenumber units).

Figure 6. Relative fluorescence intensity (□) and relative fluorescence decay time (■) of LH2 complexes from *Rb. sphaeroides* as a function of temperature. The smooth, dark curve through the data points is calculated according to eq 4. The inset shows the model scheme for the ground and excited electronic states. See the text for details.

factor on the order of 1 should be considered. This estimation not only correlates positively with the expectations discussed above but also has been confirmed recently by a simultaneous analysis of hole-burning and fluorescence line-narrowing data related to the B870 band.[32] In addition, the dual nature of the LH2 emission band has been confirmed in ref 32, supporting the assumption made above. As will be shown below, the remaining fluorescence after subtracting the RF component can be assigned to strongly coupled self-trapped (ST) excitons. The spectral independence of the lifetime beginning from ∼890 nm in Figure 4a then marks the spectral boundary beyond which only the ST spectrum is recorded.

At elevated temperatures, the wavelength dependence of the fluorescence lifetime diminishes, as was already noted (Figure 4a). The most probable explanation of this phenomenon is a temperature-induced (homogeneous) broadening of the component spectra along with the population of the higher-energy states. One might expect in this case to observe a decrease in the lifetime on the blue side of the spectrum, which is accompanied by an increase on the red side. This is exactly what can be seen in Figure 4a. It appears that the curves measured at different temperatures turn around a point in the Figure plane with approximate coordinates of 1.4 ns and 877 nm.

Fluorescence Band Shape, Intensity, and Lifetime as a Function of Temperature. Figure 5a shows fluorescence spectra at different temperatures. The two dominant trends in spectral evolution with increasing temperature evident in this Figure are a blue shift of the emission maximum and band
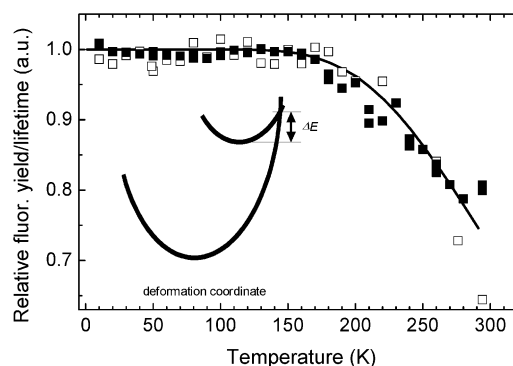
broadening (see inset of Figure 5a). A careful inspection of the band shapes at intermediate temperatures (100−160 K) reveals that the observed peak shift is largely a result of redistribution between two spectral components rather than a continuous shift of a single band. This tendency is very apparent from the second-derivative spectra presented in Figure 5b, which have the useful property of amplifying the hidden structure of the original spectra. At low temperatures up to ∼50 K, a single fluorescence band exists, and at higher temperatures, an additional band emerges from the blue side. The blue-band maximum is close to the B850 absorption band peak. Assuming that only two bands combine to form the observed fluorescence line shape, it is possible to separate their contribution, though with some uncertainty. Then the higher-energy band intensity increases gradually with temperature until at ambient temperature its contribution becomes comparable to that of the lower-energy band (data not shown).

Shown in Figure 6 is the temperature dependence of the fluorescence intensity and lifetime plotted relative to their 5 K values. The lifetime has been recorded around the low-temperature fluorescence maximum where it is least influenced by the temperature (Figure 4a). The decay kinetics, being single-exponential at low temperatures, become multiexponential above 180 K. The data points in Figure 6 then represent an average decay time.

As seen in Figure 6, both the intensity and lifetime behave similarly. The almost constant dependence between 5 and ∼180 K is followed by a small decline reaching ∼30% at room temperature. The present data are in qualitative agreement with earlier observations for LH2[17][35] and also for the B820 subunit of the LH1 antenna.[36] The parallel dependence of the fluorescence intensity and lifetime on temperature implies that the radiative decay rate of excitons is independent of temperature. This is in contrast to the disordered exciton model, which predicts[24] substantial variations in the B850 exciton lifetime due to thermal population of the higher (superradiant) exciton states unless much stronger diagonal energy disorder is present than the disorder detected experimentally.

Self-Trapped Exciton Polarons in the Disordered B850 Ring. It is apparent that the disordered exciton model in its standard form falls short in describing most of the experimental observations of this work. The same conclusion was reached earlier by analyzing exciton-state selective fluorescence data[20] as well as absorption and emission band shift rates under hydrostatic pressure.[37] In these previous studies, evidence has been provided for self-trapping of at least $k = \pm 1$ excitons in LH2 complexes at low temperatures. For this reason, the present

data will also be interpreted on the basis of the exciton self-trapping formalism, a brief description of which is included here for completeness. (See refs 20, 37, and 38 for details.)

In the adiabatic approximation, the Hamiltonian of an exciton interacting with the lattice distortion reads[21,39]

$$H = \sum_n \epsilon_n |n\rangle\langle n| + \sum_{n \neq m} t_{nm}|n\rangle\langle m| + c\sum_n q_n|n\rangle\langle n| + \frac{1}{2}\sum_n q_n^2 \quad (2)$$

Here, $|n\rangle$ and $\langle n|$ represent ket and bra vectors, respectively, of an excitation localized on site n, and matrix elements t_{nm} denote the dipole−dipole coupling energies between the pigments at sites n and m ($n \neq m$); q_n represents the local pigment ring distortion at site n, and $c \equiv \sqrt{2S\varpi}$ is the short-range excitation−lattice coupling constant, being the same for all sites. (ϖ is the mean energy of the dispersionless (optical) vibrational modes coupled to the electronic transition, and S has been defined above.) The excited-state energy ϵ_n is assumed to be a Gaussian random variable with mean ϵ_0 and variance σ. The first two terms in eq 2 represent the exciton energy, the third term represents the exciton−lattice coupling energy, and the last term is the lattice potential energy with an elastic constant taken as unity.

Bloch-type wave functions characterized by wavenumber k represent exciton states in rigid lattices without disorder (ϵ_n, q_n = const; $c = 0$). If excitation transfer is not present, then the exciton is localized on a single site and the lattice distortion lowers its energy by $S\varpi = c^2/2$, the lattice relaxation energy E_{LR}. The ratio of the lattice relaxation energy to half of the exciton bandwidth $2V = 2\max|t_{nm}|$ defines the exciton−lattice coupling constant $g = S\varpi/2V$. Stationary states of excitons in deformable and disordered lattices described by superposition $|k\rangle = \sum_n \varphi_{nk}|n\rangle$ can be obtained numerically by minimizing expectation values of the eq 2 Hamiltonian with respect to the set of local distortions $\{q_n\}$ and vector amplitudes $\{\varphi_{nk}\}$. Usually, a trial wave function with a cusp amplitude distribution is employed. This approach is not applicable here because of the small number of lattice sites and the disorder present. Disorder causes strong deviations in amplitudes for individual rings, which should be accounted for specifically.

After variationally eliminating the distortions, we found the eigenvector amplitudes $\{\tilde{\varphi}_{nk}\}$ by minimizing the expectation value of the total Hamiltonian (eq 2):

$$E_k^0(\{\tilde{\varphi}_{nk}\}) = \min\left[\sum_n\left(\epsilon_n - \frac{c^2}{2}|\varphi_{nk}|^2\right)|\varphi_{nk}|^2 + \sum_{n\neq m} t_{nm}\varphi_{nk}^*\varphi_{mk}\right]_{\varphi_{nk}=\tilde{\varphi}_{nk}} \quad (3)$$

$E_k^0(\{\tilde{\varphi}_{nk}\})$ represents the optimized ground-state energy of an exciton polaron (self-trapped exciton) composed of exciton and lattice energies $E_k + E_{LR}^{ST}$. In spectroscopic terms, this corresponds to the position of the zero-phonon line of the polaron absorption. The eigenvalue of the polaron corresponding to the emission maximum observed in fluorescence experiments is obtained from the ground-state energy by subtracting the lattice relaxation energy E_{LR}^{ST}:

$$E_k(\{\tilde{\varphi}_{nk}\}) = E_k^0\{\tilde{\varphi}_{nk}\} - \frac{c^2}{2}\sum_n|\varphi_{nk}|^4 \quad (4)$$

It is important to realize that the functional (eq 3) is nonlinear in amplitudes φ_{nk}; therefore, its minimum depends on the initial-state amplitude vector. This is why both energy and amplitudes
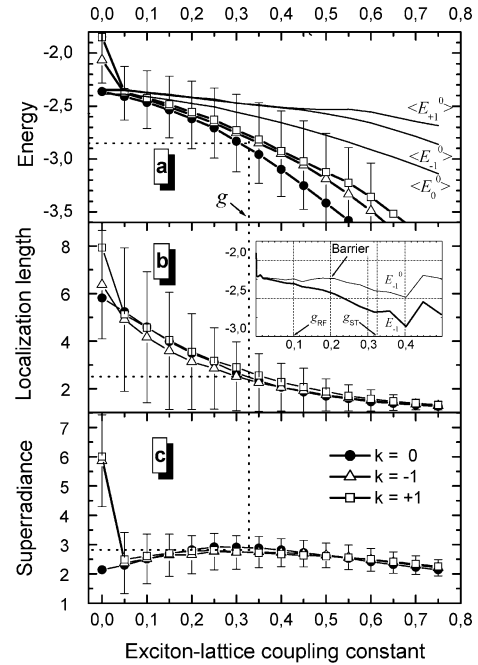

Figure 7. Ensemble-averaged (more than 1000 samples) dependence of the ground-state characteristics for exciton polarons seeded by free-exciton states $k = 0, \pm1$ as a function of the exciton−lattice coupling constant at zero temperature: (a) E_k^0 as well as E_k state energies; (b) localization length (defined as the inverse participation ratio, $L_k = (\sum_n|\tilde{\varphi}_{nk}|^4)^{-1}$); (c) superradiance enhancement factor, $F_k = \sum_{nm}(\mu_n\mu_m)\tilde{\varphi}_{nk}^*\tilde{\varphi}_{mk}$ (μ_n is the transition dipole moment vector for the nth pigment). The inset shows E_k^0 and E_k energies of the $k = -1$ state for a single disorder realization. Ring aggregates have been constructed according to the known B850 structure with the relative diagonal disorder standard deviation $\sigma/V = 0.6$. Exciton coupling energy accounting for all 18 sites in the ring is calculated in a dipole−dipole approximation. The bars refer to the width of the ensemble distribution for the $k = -1$ state.

are labeled according to the free-exciton momentum k. The results of direct numerical calculations for the three lowest excitons of the B850 ring aggregate of LH2 are presented in Figure 7. The relative diagonal disorder $\sigma/V = 0.6$, which was required to describe the LH2 absorption spectrum[19] well, was applied.

The main conclusions from these simulations can be formulated as follows: (i) All of the exciton states self-trap because of coupling to lattice vibrations. (ii) The final (self-trapped) fluorescence states reached after the self-trapping relaxation depend on the initial (absorbing or seed) states. (iii) The self-trapped exciton energy decreases with increases in the exciton−lattice coupling constant g. (iv) The coexistence of large and small self-trapped excitons takes place for all but the $k = 0$ states. The latter result is not apparent from the disorder-averaged plots in Figure 7a because of large fluctuations (see the bars). However, for a particular realization of disorder, the existence of an energetic barrier separating weakly (denoted by exciton−lattice coupling constant g_{RF}) and strongly (g_{ST}) coupled excitons is confirmed, as shown in the inset of Figure 7 for the expectation value E_k^0 that corresponds to the $k = -1$ state. It has been verified that such coexistence is present in 35−40% cases of disorder realizations and naturally explains the dual nature of the fluorescence band discussed above (Figure 4b).

A proper scaling is needed for the quantitative application of model results in Figure 7. It assumes a knowledge of the three basic parameters comprising the interpigment coupling

V, diagonal disorder variance σ, and exciton−lattice coupling constant g. The optimal parameter set was searched by fitting to the whole set of available experimental data, including the steady-state selective and nonselective absorption/emission spectra and their anisotropy dependences. The details of this extensive search procedure will be published elsewhere. Here, we limit ourselves to pointing out the optimal parameter values obtained: $V \approx 430$ cm^{-1}, $\sigma \approx 0.6$ V, and g ≈ 0.33. The transition-energy difference between the bacteriochlorophylls bound to α- and β-helixes was fixed at $\Delta \approx 0.8$ V.

One now gets from V and g that $E_{LR} \approx 284$ cm^{-1}. We recall that E_{LR} refers to the limiting lattice relaxation energy when the exciton is localized on a single site. The extended exciton feels much less phonon field than does the localized excitation. For the delocalized excitations, the intensity of the one-phonon sideband relative to that of the zero-phonon line is reduced by a factor of $(\varpi 2dV)^{d/2}$ (d, the dimensionality of the lattice, is equal to 1 here);[40] therefore, the observable lattice relaxation energy is generally less than E_{LR}. As we have seen (Figure 4b), the experimental exciton−lattice relaxation energy for the red subband is $E_{LR}^{ST} \approx 146$ cm^{-1} (calculated as the energy difference between the inhomogeneous distribution function at 864.9 nm and the maximum of the red fluorescence subband at 876.0 nm). This value compares favorably with the calculated ∼140-cm^{-1} gap between the ensemble average of expectation energies and emission maxima in Figure 7a at $g \approx 0.33$. The corresponding ensemble-averaged localization length of self-trapped excitons is between 2 and 3 (Figure 7b). (The exciton size is traditionally measured in lattice constants or in the number of molecular sites.) This number, being fully consistent with the dimeric structure of LH2, is similar to the one obtained from the analysis of exciton annihilation data.[41] Also, the calculated superradiance enhancement ratio shown in Figure 7c and equal to 2.8 is identical to the ratio estimated from the integral fluorescence yield and lifetime measurements.[35]

As for the apparent coupling parameter, g_{RF}, characterizing resonant fluorescence, it can be estimated using the mean frequency $\bar{\omega} \approx 80$ cm^{-1} and the Huang−Rhys factor $S_{RF} \approx 0.8-1.0$ determined recently from the resonant fluorescence line-shape analysis.[32] It results in the apparent lattice relaxation energy $E_{LR}^{RF} = S_{RF}\bar{\omega} \approx 60-80$ cm^{-1} and the exciton lattice coupling $g_{RF} \approx 0.1$. At this g value, the ensemble-averaged localization length of self-trapped excitons is almost twice as large as in the case of $g \approx 0.33$, which explains the more suppressed one-phonon sideband and, consequently, the smaller lattice relaxation energy observed.

The B870 band may now be interpreted as being related to self-trapped excitons weakly coupled to the surrounding lattice. The corresponding relaxed exciton size, $N_{RF} \approx 4-5$ (Figure 7b), allows this state to be classified as a large-radius self-trapped exciton. This is in contrast to the self-trapped exciton states giving rise to the red fluorescence subband, which are of considerably smaller radius ($N_{ST} \approx 2-3$).

A simplified configuration coordinate diagram shown in Figure 8 illustrates the issue. Represented in this Figure are the diabatic potential energy curves corresponding to the $k = 0$, ±1 free-exciton seed states and the two main self-trapped exciton states discussed in the present paper. The term "free exciton" is used here in contrast to "self-trapped exciton". Disordered excitons are, of course, partially localized even in rigid aggregates (see ref 19 and Figure 7b). The approximate lattice relaxation energies shown for the ground-state potential have been taken as in the experiment (Figure 4b). The arrows
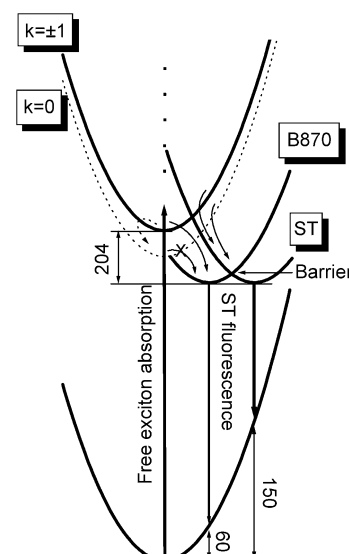

Figure 8. Configuration coordinate diagram illustrating the self-trapping of excitons in the B850 aggregate. Only the $k = 0$, ±1 free-exciton states are explicitly shown. The straight and curved arrows represent optical transitions and the main relaxation channels, respectively. The numbers indicate approximate energy differences in wavenumbers. See the text for details.

show the main relaxation channels deduced from the comparison of experiment to model calculations.

The analysis of data in Figure 7 suggests that the $k = 0$ free-exciton state may relax into the small-radius self-trapped exciton state if it is excited at the far-red edge of the absorption spectrum. We have recently confirmed these model predictions by measuring the energy gap between spectrally narrow laser excitation and the fluorescence maximum as a function of excitation wavelength. This is the same dependence as in ref 17 but extended toward lower energies (data not shown). As seen, the gap initially diminishes with the wavelength, reaches a minimum of 119 ± 5 cm^{-1} at the blue subband region, and starts to increase beyond it. At ∼890 nm (the same wavelength from which the spectral independence of the fluorescence lifetime in Figure 4a is observed), the gap is ∼155 ± 5 cm^{-1}, close to the relative red subband shift shown in Figure 4b. This once again demarks the spectral boundary beyond which only the red subband contributes to the LH2 fluorescence, providing a natural explanation for the recorded equality of the gap and the relative red subband shift. Because there is no barrier separating different self-trapped states related to the $k = 0$ free-exciton state, no relaxation into the large-radius self-trapped exciton state is possible (emphasized by the crossed arrow in Figure 8).

Figure 8 also helps to explain the complex temperature dependence of fluorescence band shapes in Figure 5. The blue satellite band emerging at higher temperatures is obviously due to thermal population of the $k = \pm 1$ free-exciton states at the expense of the self-trapped exciton populations. The parallel fluorescence yield and lifetime curves, such as those shown in Figure 6, were earlier interpreted as evidence of the temperature independence of the exciton coherence size in the B850 ring.[35] This analysis assumed that the coherence size was limited by large static disorder. The present data elaborate on this interpretation in two important aspects. For the majority of excitons, the main factor limiting the size of the relaxed exciton is dynamic rather than static disorder. It also appears that the observed constancy of the exciton radiative rate may be accidental. The $k = \pm 1$ free-exciton states populated at higher

temperatures lead to an increased rate, and that of $k = 0$, to a decreased rate partially compensating the former result. Thermally activated multiphonon processes may in turn overwhelm both effects.

The parallel fluorescence intensity and lifetime curves in Figure 6 imply that the temperature dependence that is observed is purely of a radiationless nature. Provided that the relaxed excitons in LH2 complexes are essentially localized over the whole temperature range studied, the energy-gap law for radiationless transitions should apply.[42] In the strong-coupling limit, the nonradiative decay rate constant is given by

$$k_{NR}(T) = \frac{A}{(k_B T_{eff})^{1/2} \exp(-\Delta E/k_B T_{eff})} \quad (5)$$

In eq 5, A is a constant, ΔE is the activation energy (see inset of Figure 6), and T_{eff} is the effective temperature defined as $k_B T_{eff} = (^1/_2)\varpi \coth(\varpi/2k_B T)$. A fit drawn with a solid smooth line in Figure 6 is proportional to $k_R/(k_R + k_{NR}(T))$, where k_R is the radiative decay rate constant of the excited state, independent of temperature. The radiative decay rate constant has been fixed at $k_R \approx (6.6 \text{ ns})^{-1}$, taking into account the 16.6-ns radiative lifetime of an isolated Bchl molecule[35] and the average superradiance enhancement factor in the B850 ring equal to $\sim$2.8 (see Figure 7c.) Ignoring possible differences between vibrational frequencies strongly coupled to different radiative and nonradiative transitions, the effective frequency is taken as $\varpi \approx 60 \text{ cm}^{-1}$, consistent with the phonon sideband maximum found for the B870 exciton states.[32] This leaves A and ΔE as the only free parameters. As seen, a reasonable fit is obtained with $A \approx 170 \text{ cm}^{-1/2}/\text{ns}$ and $\Delta E \approx 1500 \text{ cm}^{-1}$. To relate the configuration coordinate diagrams in Figures 6 and 8, one can think of a single excited state in the inset of Figure 6 as corresponding to a mixture of the two localized states shown in Figure 8. This approximation is definitely valid at temperatures greater than 100 K.

Concluding Remarks

We have thus verified that the absorbing and emitting states in the B850 aggregate of the LH2 complex are dynamically separated by structural relaxation (self-trapping) caused by interplay between the electronic and nuclear degrees of freedom. The excitons self-trap not only at low temperatures, as previously suggested,[17] but also over the whole temperature range up to physiological temperatures because of substantial self-trapped exciton binding energy comparable with the thermal excitation energy, $k_B T$, at room temperature (Figure 8). A similar conclusion had been reached earlier on the basis of the analysis of the temperature dependence of high-pressure-induced absorption and fluorescence band shifts.[37] These findings call for a revision of current concepts concerning the origin of the LH2 antenna optical spectra. The fluorescence at all temperatures is due mainly to self-trapped excitons. The coexistence of large-radius and small-radius exciton polarons is confirmed, probably for the first time in disordered 1D molecular aggregates. The self-trapping relaxation reflects itself also in a modified absorption spectrum,[43] especially around the long-wavelength tail. A fraction ($\sim$45% at 871.6 nm, considering $S_{RF} \approx 0.8$) of the absorption spectrum of LH2 that is subject to hole burning is due to large-radius self-trapped excitons. We notice that the zero-phonon lines associated with self-trapped exciton states have been observed in β-perylene crystals.[44] The rest of the long-wavelength absorption spectrum that survives hole burning belongs to the small-radius self-trapped excitons. Because the

fractional absorbance change at the burn wavelength is determined by $\exp(-S)$, it is apparent why only the holes corresponding to the large-radius self-trapped exciton states could be observed and not those related to the small-radius states. In the latter case, the holes are expected to be approximately 1.5 orders of magnitude weaker than in the former case.

To the extent that the fluorescence at low temperatures is from the self-trapped states localized on molecular dimers, the fluorescence can be assigned to excimers. As it is well known, excimers refer to dimers that are formed in the excited state (see ref 45 for a review). The excimer idea is supported by the sum rule of distortions

$$\sum_n q_n = -c \quad (6)$$

which stems from the Hamiltonian (eq 2) variational procedure. In the case of a dimer, for example, eq 6 suggests a closer approach of molecules after excitation (i.e., excimer formation). Microscopically, the excimer interaction is attributed to the configurational mixing of neutral exciton and charge-transfer states. This not only provides a natural explanation of the relatively strong exciton−phonon coupling that is observed but also substantiates the larger pressure sensitivity of the emission spectra compared to that of the absorption spectra,[37] though the charge-transfer states have not been explicitly considered in our modeling.

One can identify two relaxation paths leading to self-trapped exciton states at nonresonant excitation: the so-called direct and sequential channels (Figure 8). The latter route is mediated by conventional weak-coupling inter-exciton-state relaxation to the bottom of the free-exciton band, which most probably is the dynamical bottleneck of the process. An important question of excitation energy branching between direct and sequential relaxation pathways then arises. This still remains to be studied quantitatively. However, from the present study, it is safe to conclude that the self-trapping relaxation clearly dominates the inter-exciton-state relaxation in the B850 aggregate. A similar situation is present in pyrene crystals, a model representative of quasi-1D molecular systems.[46]

We believe that this novel analysis also helps us to understand the LH2 electroabsorption and electrofluorescence (Stark spectroscopy) data from this complex.[47,48] The most puzzling electric-field-induced effect not interpreted so far is an extra weak absorption band appearing at the long-wavelength absorption tail, about 250 cm^{-1} below the B850 absorption peak. A decrease in fluorescence intensity spectrally correlated with increased absorption was observed. Our model offers a qualitative explanation for both effects. As can be seen in Figure 8, the ST state is located 248−250 cm^{-1} below the B850 absorption peak. The electric field evidently redistributes exciton relaxation pathways and promotes the one that directly leads to the ST state. The concomitant fluorescence reduction is then simply due to increased fluorescence (re)absorption at this wavelength (see also Figure 2a for reference).

The broad fluorescence band of self-trapped excitons considerably improves the energy resonance between different antenna complex spectra as well as that between the reaction center and antenna complexes. However important, self-trapping seems to be only a part of nature's strategy to promote efficient light harvesting in the photosynthetic membrane. As seen in Figure 5, the quasi-free-exciton fluorescence also helps in gaining some extra width to the fluorescence spectrum at elevated temperatures.

References and Notes

(1) van Amerongen, H.; Valkunas, L.; van Grondelle, R. *Photosynthetic Excitons*; World Scientific: Singapore, 2000; pp 590 .

(2) Freiberg, A. In *Anoxygenic Photosynthetic Bacteria*; Blankenship, R. E., Madigan, M. T., Bauer, C. E., Eds.; Kluwer Academic Publishers: Dordrecht, The Netherlands, 1995; Vol. 2, pp 385−398

(3) McDermott, G.; Prince, S. M.; Freer, A. A.; Hawthornthwaite-Lawless, A. M.; Papiz, M. Z.; Cogdell, R. J.; Isaacs, N. W. *Nature* **1995**, *374*, 517−21.

(4) Koepke, J.; Hu, X.; Muenke, C.; Schulten, K.; Michel, H. *Structure* **1996**, *4*, 581−597.

(5) Sundström, V.; Pullerits, T.; van Grondelle, R. *J. Phys. Chem. B* **1999**, *103*, 2327−2346.

(6) van der Laan, H.; Schmidt, T.; Visschers, R. W.; Visscher, K. J.; van Grondelle, R.; Völker, S. *Chem. Phys. Lett.* **1990**, *170*, 231−238.

(7) Reddy, N. R. S.; Cogdell, R. J.; Small, G. J. *Photochem. Photobiol.* **1991**, *57*, 35−39.

(8) Tietz, C.; Chekhlov, O.; Dräbenstedt, A.; Schuster, J.; Wrachtrup, J. *J. Phys. Chem. B* **1999**, *103*, 6328−6333.

(9) van Oijen, A. M.; Ketelaars, M.; Köhler, J.; Aartsma, T. J.; Schmidt, J. *Science* **1999**, *285*, 400−402.

(10) Sauer, K.; Cogdell, R. J.; Prince, S. M.; Freer, A.; Isaacs, N. W.; Scheer, H. *Photochem. Photobiol.* **1996**, *64*, 564−576.

(11) Dracheva, T. V.; Novoderezhkin, V. I.; Razjivin, A. P. *FEBS Lett.* **1996**, *387*, 81−84.

(12) Reddy, N. R. S.; Picorel, R.; Small, G. J. *J. Phys. Chem.* **1992**, *96*, 6458−6464.

(13) Jimenez, R.; Dikshit, S. N.; Bradforth, S. E.; Fleming, G. R. *J. Phys. Chem.* **1996**, *100*, 6825−6834.

(14) Wu, H.-M.; Rätsep, M.; Lee, I.-J.; Cogdell, R. J.; Small, G. J. *J. Phys. Chem. B* **1997**, *101*, 7654−7663.

(15) Freiberg, A.; Jackson, J. A.; Lin, S.; Woodbury, N. W. *J. Phys. Chem. A* **1998**, *102*, 4372−4380.

(16) Freiberg, A.; Timpmann, K.; Lin, S.; Woodbury, N. W. *J. Phys. Chem. B* **1998**, *102*, 10974−10982.

(17) Timpmann, K.; Katiliene, Z.; Woodbury, N. W.; Freiberg, A. *J. Phys. Chem. B* **2001**, *105*, 12223−12225.

(18) Visschers, R. W.; Germeroth, L.; Michel, H.; Monshouwer, R.; van Grondelle, R. *Biochim. Biophys. Acta* **1995**, *1230*, 147−154.

(19) Freiberg, A.; Timpmann, K.; Ruus, R.; Woodbury, N. W. *J. Phys. Chem. B* **1999**, *103*, 10032−10041.

(20) Freiberg, A.; Rätsep, M.; Timpmann, K.; Trinkunas, G. *J. Lumin.* **2003**, *102−103*, 363−368.

(21) Rashba, I. E. In *Excitons*; Sturge, M. D., Ed.; North-Holland: Amsterdam, 1982; pp 543−602.

(22) Meier, T.; Zhao, Y.; Chernyak, V.; Mukamel, S. *J. Chem. Phys.* **1997**, *107*, 3876−3893.

(23) Chernyak, V.; Meier, T.; Tsiper, E.; Mukamel, S. *J. Phys. Chem. A* **1999**, *103*, 10294−10299.

(24) Zhao, Y.; Meier, T.; Zhang, W. M.; Chernyak, V.; Mukamel, S. *J. Phys. Chem. B* **1999**, *103*, 3954−3962.

(25) Polivka, T.; Pullerits, T.; Herek, J. L.; Sundström, V. *J. Phys. Chem. B* **2000**, *104*, 1088−1096.

(26) Damjanovic, A.; Kosztin, I.; Kleinekathöfer, U.; Schulten, K. *Phys. Rev. E* **2002**, *65*, 031919−031943.

(27) Timpmann, K.; Woodbury, N. W.; Freiberg, A. *J. Phys. Chem. B* **2000**, *104*, 9769−9771.

(28) *Dynamic Light Scattering: The Method and Some Applications*; Brown, W., Ed.; Oxford University Press: Oxford, U.K., 1993.

(29) Freiberg, A.; Saari, P. *IEEE J. Quantum Electron.* **1983**, *QE-19*, 622−630.

(30) Wu, H.-M.; Rätsep, M.; Jankowiak, R.; Cogdell, R. J.; Small, G. J. *J. Phys. Chem. B* **1997**, *101*, 7641−7653.

(31) Hayes, J. M.; Gillie, J. K.; Tang, D.; Small, G. J. *Biochim. Biophys. Acta* **1988**, *932*, 287−305.

(32) Rätsep, M.; Freiberg, A. *Chem. Phys. Lett.* **2003**, *377*, 371−376.

(33) Kennis, J. T. M.; Streltsov, A. M.; Permentier, H.; Aartsma, T. J.; Amesz, J. *J. Phys. Chem. B* **1997**, *101*, 8369−8374.

(34) Sebban, P.; Jolchine, G.; Moya, I. *Photochem. Photobiol.* **1984**, *39*, 247−253.

(35) Monshouwer, R.; Abrahamsson, M.; van Mourik, F.; van Grondelle, R. *J. Phys. Chem. B* **1997**, *101*, 7241−7248.

(36) Helenius, V.; Monshouwer, R.; van Grondelle, R. *J. Phys. Chem. B* **1997**, *101*, 10554−10559.

(37) Timpmann, K.; Ellervee, A.; Kuznetsov, A.; Laisaar, A.; Trinkunas, G.; Freiberg, A. *J. Lumin.* **2003**, *102−103*, 220−225.

(38) Timpmann, K.; Trinkunas, G.; Katiliene, Z.; Woodbury, N. W.; Freiberg, A. *PS2001 Proceedings: 12th International Congress on Photosynthesis*; CSIRO Publishing: Melbourne, Australia, 2001; pp S1−018. Available at http://www.publish.csiro.au/ps2001.

(39) Holstein, T. *Ann. Phys.* **1959**, *8*, 325−342.

(40) Ueta, M.; Kanzaki, H.; Kobayashi, K.; Toyozawa, Y.; Hanamura, E. In *Springer Series of Solid-State Sciences*; Cardona, M., Fulde, P., von Kitzling, K., Queisser, H.-J., Eds.; Springer: Berlin, 1986; pp 530.

(41) Trinkunas, G.; Herek, J. L.; Polivka, T. V.; Sundström, V.; Pullerits, T. *Phys. Rev. Lett.* **2001**, *86*, 4167−4170.

(42) Englman, R.; Jortner, J. *J. Mol. Phys.* **1970**, *18*, 145−164.

(43) Sumi, H. *J. Phys. Soc. Jpn.* **1975**, *38*, 825−835.

(44) Matsui, A.; Mizuno, K.; Nishimura, H. *J. Phys. Soc. Jpn.* **1984**, *53*, 2818−2827.

(45) Birks, J. B. *Rep. Prog. Phys.* **1975**, *38*, 903−974.

(46) Furukawa, M.; Mizuno, K.; Matsui, A.; Tamai, N.; Yamazaki, I. *Chem. Phys.* **1989**, *138*, 423−432.

(47) Gottfried, D. S.; Stocker, J. W.; Boxer, S. G. *Biochim. Biophys. Acta* **1991**, *1059*, 63−75.

(48) Beekman, L. M. P.; Steffen, M.; van Stokkum, I.; Olsen, J. D.; Hunter, C. N.; Boxer, S. G.; van Grondelle, R. *J. Phys. Chem. B* **1997**, *101*, 7284−7292.